Numerical Computation of Spatially Developing Flows by Full-Multigrid Technique

A Thesis

Submitted For the Degree of

MASTER OF SCIENCE (ENGINEERING)

in the Faculty of Engineering

by

Kirti Chandra Sahu

ENGINEERING MECHANICS UNIT
JAWAHARLAL NEHRU CENTRE FOR ADVANCED SCIENTIFIC
RESEARCH
Bangalore − 560 064

JULY 2003

To my brother Mr. Surya Narayana Sahu

DECLARATION

I hereby declare that the matter embodied in the thesis entitled "**Numerical Computation of Spatially Developing Flows by Full-Multigrid Technique**" is the result of investigations carried out by me at the Engineering Mechanics Unit, Jawaharlal Nehru Centre for Advanced Scientific Research, Bangalore, India under the supervision of Prof. Rama Govindrajan and that it has not been submitted elsewhere for the award of any degree or diploma.
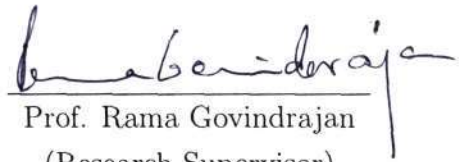
In keeping with the general practice in reporting scientific observations, due acknowledgement has been made whenever the work described is based on the findings of other investigators.

Kirti Chandra Sahu
_____
Kirti Chandra Sahu

CERTIFICATE

I hereby certify that the matter embodied in this thesis entitled "**Numerical Computation of Spatially Developing Flows by Full-Multigrid Technique**" has been carried out by Mr. Kirti Chandra Sahu at the Engineering Mechanics Unit, Jawaharlal Nehru Centre for Advanced Scientific Research, Bangalore, India under my supervision and that it has not been submitted elsewhere for the award of any degree or diploma.

Prof. Rama Govindrajan

(Research Supervisor)

Acknowledgements

I am indebted to Prof. Rama Govindrajan for her valuable contributions and guidance at every stage of this work, and indeed for teaching me what research is all about; I am fortunate to have her as my advisor.

I am grateful to Prof. Roddam Narasimha for his valuable suggestions.

I am extremely grateful to Dr. K.R.Sreenivas and Dr. Meheboob Alam for their constant support and encouragement.

It is a pleasure to thank Prof. S.P. Vanka for giving me a foundation in Computational Fluid Dynamics, for his keen interest in the work and many helpful suggestions to accelerate the rate of convergence. I thank him for sharing his multigrid algorithm with us.

I thank Dr. N. Balakrishan and Dr. Josheph Mathew for their valuable advice.

I thank all my colleagues at JNCASR, especially I thank Mr. N.Vinod and Mr. A.Sameen for their support at every stage of my work. I also thank Mr. Subrata pal and Mr. Joydeep Bhattacharjee for their help with TeX and other matters.

I thank Dr. Umesh V Waghmare for allowing me to use all the complab facilities. I also thank the office staff of JNCASR for their prompt and

generous help.

Finally I thank my parents for allowing me to continue my studies.

Synopsis

The instability of spatially developing laminar flows, such as that through converging/diverging channels, is often fundamentally different from flows that do not vary downstream. Another class of flows whose stability and transition behaviour is not well understood is pulsatile flows. In most laminar flows which fall under these categories, it is not possible to obtain the basic flow profiles analytically. The aim of this thesis is to develop codes which will compute the basic flow for two dimensional and axisymmetric geometries. A long-term objective is to understand the transition to turbulence in such flows. The Navier-Stokes equations in the vorticity and streamfunction formulation have been solved for computing the mean flow. Two types of spatially developing flows have been considered, namely, flow in a divergent channel and axisymmetric flow in a divergent pipe. The code can handle unsteady problems, but has been used up to now to solve a pseudo-unsteady problem to obtain steady state solutions.

The Gauss-Seidel iteration method was found to be alarmingly slow in solving the elliptic streamfunction and vorticity equation with vorticity as a source term. To increase the rate of convergence, a multigrid technique has been implemented. Algorithms like Jacobi or Gauss-Seidel are local because

the new value for the solution at any lattice site depends only on the value of the previous iterate at neighbouring points. The basic idea behind multigrid technique is to reduce long wavelength error components rapidly by updating blocks of grid points. We used a simple V-cycle for the present algorithm. For Poisson equation with 128x128 number of grids, using six multigrid levels, it was found that multigrid technique is about a hundred times faster then the Gauss-Seidel method.

The present code has been tested with a number of experimental and theoretical bench-mark results for the developing flow in a channel and a flow in a backward-facing step. The multigrid algorithm has been compared with the Gauss-Seidel iteration method for the Poisson equation. With the present code, we were able to simulate the separated flow with reattachment for a divergent channel and pipe, with straight exit portions, for different angles of divergence and Reynolds number. As an analytical solution is not possible for such kind of flows, with large angle of divergence, solution of full Navier-Stokes equation is required. The code in the present form can be used for this purpose. In summary, we now have the capability of studying the stability of a wide class of spatially developing and time-periodic flows.

Nomenclature

l	Number of multigrid level.
Re	Reynolds number.
r	Radius of the axisymmetric pipe.
t	Time.
u	Streamwise velocity.
v	Vertical velocity.
U_i	Centerline velocity at the inlet.
U	Local centerline velocity.
x	Coordinate in the streamwise direction.
y	Coordinate in the normal direction.
$\zeta, \ \eta$	Transformed coordinate system.
ψ	Streamfunction.
ω	Vorticity.
ω_{rsd}	Vorticity residual.

Contents

List of Figures

Chapter 1

Introduction

1.1 Background

Flow is generally laminar at low Reynolds number. When the Reynolds number increases, flows undergo a remarkable transition from the laminar to turbulent regime. The origin of turbulence and the accompanying transition from laminar to turbulent flow is of fundamental importance for the whole science of fluid mechanics. Theoretical investigations of flow stability are based on the assumption that laminar flows are affected by certain small disturbances. If the disturbances decay with time, the mean flow is considered stable; on the other hand, if the disturbances grow with time, the mean flow is unstable, and there exists the possibility of transition to turbulence. The objective of the stability theory is to predict the value of critical Reynolds number for a prescribed mean flow. Spatially developing flows have certain special features. They are:

1. Sensitivity of stability to flow parameters.

2. Non-zero normal velocity.

Because of these features a non-parallel stability analysis is required. For this the mean flow has to be first computed very accurately. The objective of the present work is to compute the mean flow for selected spatially developing flows, with the long term aim of studying instabilities, separation and unsteady behavior. The Navier-Stokes equation in the form of vorticity and streamfunction formulation have been solved in the present work. The solution procedure largely depends on the nature of these partial differential equations. Broadly, partial differential equations can be classified as follows [2].

i) Parabolic equations:

Parabolic equations have only one characteristic direction, i.e, the information is propagated in one direction. Knowing the initial and boundary condition, it is possible to march in that direction.

ii) Hyperbolic equations:

Hyperbolic equations have two real characteristic curves through the point of interest. The significance of these characteristics curves is that information at the point of interest influences only the region between the two characteristics curves. The computation of flow fields that are governed by hyperbolic equations is again possible by space marching.

iii) Elliptic equations:

For elliptic equations, there are no limited regions of influence or domains of dependence; rather, information is propagated in all directions. Unlike parabolic and hyperbolic equations, a space marching solution is not possible. For this reason, problems involving elliptic equations are frequently called

jury problems, because the solution within the domain depends on the total domain, so boundary conditions must be applied over the entire boundary. The boundary conditions can take the following forms :

a) A specification of the dependent variables u and v along the boundary. This type of boundary condition is called the Dirichlet condition.

b) A specification of derivatives of the dependent variables, such as $\partial u/\partial x$, along the boundary. This type of boundary condition is called Neumann condition.

c) A mix of both Dirichlet and Neumann conditions.

1.2   Some spatially developing flows

1.2.1   Flow in a convergent/divergent channel

For slowly varying flow in a divergent channel, with the quasi-parallel assumption Eagles [1,3,4] assumed that stability at some point depends only in the local properties of the flow, i.e. the local profile, Reynolds number, etc. He described a steady, two-dimensional, symmetric flow wedge-shaped channel of divergence angle $2k$ and the volumetric flow rate 2M. He used the modified polar co-ordinates in the calculation.

$$\zeta = k^{-1}\ln(kr), \quad \eta = \phi/k,$$

where r and ϕ are the usual polar co-ordinates. He used the following non-dimensional vorticity equation.

$$\left[D^2 - (Re)e^{2k\zeta}\frac{\partial}{\partial\tau} - Re\left(\frac{\partial\psi}{\partial\eta}\frac{\partial}{\partial\zeta} - \frac{\partial\psi}{\partial\zeta}\frac{\partial}{\partial\eta}\right)\right][e^{-2k\zeta}D^2\psi] = 0,$$

where $Re = M/\mu$ is the Reynolds number and μ is the kinematic viscosity.
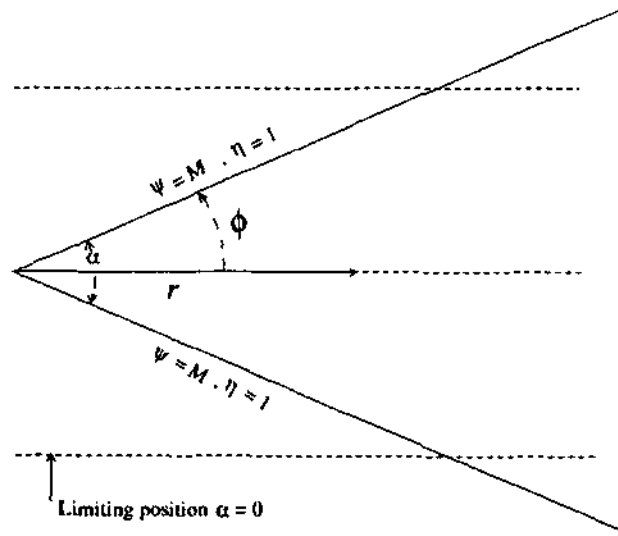
Figure 1.1: Schematic diagram for wedge shape channel

$D^2 \equiv \partial^2/\partial\zeta^2 + \partial^2/\partial\eta^2$ and $t = (b^2/M)\tau$, b is a real constant with the dimension of length. Using this velocity profile, Eagles conducted a stability analysis with the parallel flow assumption. Fig.(1.2) gives the critical Reynolds numbers for different angles of divergence from computations using Eagles equation for the velocity profile. It is seen that spatial development, though small, has a very large effect on stability.
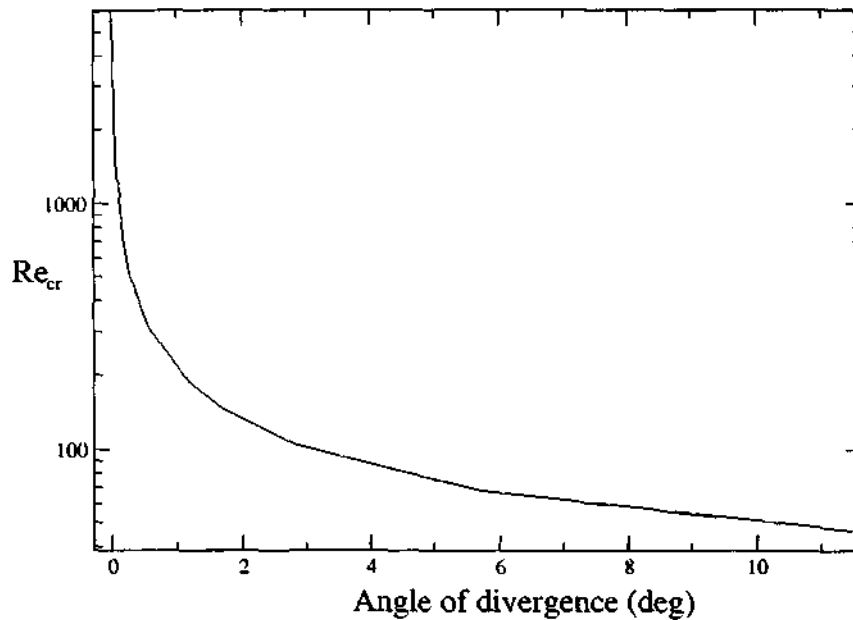
Figure 1.2: Critical Reynolds number Vs divergence by Eagles [1]

1.3 A sketch of the present work

For studying the stability, the basic flow should be known accurately first. Flows through convergent-divergent geometries are examples of a large class of spatially developing flows where the basic flow is not possible to obtain analytically. The numerical solution also often prove to be very time-consuming to obtain. The boundary conditions, especially at the outlet are often difficult to prescribe. The aim of this thesis is to develop a capability to compute such flows. The streamfunction and vorticity equations have been used in the present work. Algorithms like Jacobi or Gauss-Seidel were found to be alarmingly slow in solving the elliptic streamfunction and vorticity

equation with vorticity as a source term. The reason for this was that accuracy at the outlet boundary necessitated the use of very long domains. To accelerate the rate of convergence, a multigrid technique technique has been implemented, and it was found that multigrid technique is about a hundred times faster then the Gauss-Seidel method.

1.3.1 Flow in a divergent channel

For boundary layer flows, like flow over a flat plate, the variation in the streamwise direction is much less than the variation in the spanwise direction, i.e. $\partial/\partial x \ll \partial/\partial y$, So the term $\partial^2/\partial x^2$, being of even higher order than $\partial/\partial x$, can be neglected in the above equations. Eagles [1] investigated the stability of slowly varying flow in a divergent channel. Using a boundary layer type of approximation, he neglected the $\partial^2/\partial x^2$ term while calculating the mean flow. For extremely small angles of divergence this approximation is valid, but even for moderate angles of divergence the $\partial^2/\partial x^2$ term can not be neglected.

The goal of the present work is to solve the full Navier-Stokes equation without neglecting any term. The steady state Navier-Stokes equations are elliptic in nature. So, as discussed above, space marching is not possible. Hence even to attain a steady state, a pseudo transient term was included and time marching was done till steady state was reached. As the present work is limited to two-dimensional flows, it is often desirable to introduce the vorticity and stream function as dependent variables.

The fluid flow is solved on a Cartesian coordinate system based on the

stream function and vorticity approach. This code can be use for steady and unsteady flow. This is discussed in chapter 2.

1.3.2 Axisymmetric flow

For axisymmetric flows, there is no variation in the θ direction and $u_\theta = 0$ in cylindrical form of the Navier-Stokes and vorticity equation. In this case also it is desirable to use the stream function and vorticity approach. The use of finite difference method to solve the axisymmetric flow in a complex geometry, like a convergent-divergent pipe, is facilitated by a transformation of coordinates. In the same way as the divergent channel, a finite difference code was developed to solve the laminar, incompressible axisymmetric flow. This is discussed in chapter 3.

Chapter 2

Flow in a Divergent Channel

2.1 Summary

Consider a two dimensional, incompressible, steady flow in the geometry as shown in fig.(2.1). It consists of a parallel channel at the entry, followed by a divergent section, with a straight exit section, which is much longer then the divergent section. A long parallel exit section is taken in order to get parabolic flow at the outlet. For 2D flows it is convenient to use the vorticity and streamfunction equations as the governing equations. The streamwise diffusion term $\partial^2/\partial x^2$ cannot in general be neglected, which makes the equation elliptic. For this type of problem it is impossible to march in the x-direction, as already discussed in sect.1.3.1. So even for the steady problem, a pseudo transient term was included, and iterations were performed till steady state was reached. The fluid flow was solved for a transient, constant-density flow using a transformed coordinate system based on

the streamfunction and vorticity [5]. The continuity and momentum equations were inherently imbedded in the streamfunction and vorticity approach. This code can be use for steady and unsteady flows.

2.2   Governing Equations

$$\omega = \left(\frac{\partial^2 \psi}{\partial x^2} + \frac{\partial^2 \psi}{\partial y^2}\right),\tag{2.1}$$

$$\frac{\partial \omega}{\partial t} + \frac{\partial(u\omega)}{\partial x} + \frac{\partial(v\omega)}{\partial y} = \frac{1}{Re}\left(\frac{\partial^2 \omega}{\partial x^2} + \frac{\partial^2 \omega}{\partial y^2}\right),\tag{2.2}$$

$$u = \frac{\partial \psi}{\partial y}, \quad v = -\frac{\partial \psi}{\partial x}.\tag{2.3}$$

These are non-dimensional equations. All the variables have been non-dimensionalized as follows [6],

$$u = \frac{u_d}{U}, \quad v = \frac{v_d}{U}, \quad x = \frac{x_d}{L}, \quad y = \frac{y_d}{L}, \quad \omega = \frac{\omega_d}{\omega_0}, \quad \psi = \frac{\psi_d}{\psi_0}$$

$$\tag{2.4}$$

where U is the centerline velocity at the inlet. L is the half channel width at the entry, ψ_0 and ω_0 are the values of the streamfunction and vorticity respectively at the wall in the inlet section. The 'd' stands for a dimensional quantity.

2.3   Transformation of coordinate system

The use of a finite difference method to solve the flow in such a geometry is facilitated by a transformation of coordinates [2]. The following is the required transformation.

$$\zeta = x,$$

$$\eta = \frac{y}{f(x)}.$$

(2.5)

$f(x)$ is the function of the boundary. The half channel width at the beginning of the channel has been taken as the length scale.
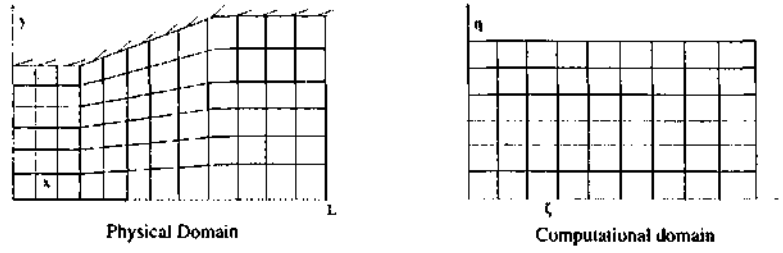
Figure 2.1: Schematic diagram of divergent channel

Fig.(2.1) is not to scale, in the geometry we have considered, the divergent part is much shorter than the straight exit part. A long straight section is provided to enable the exit flow to be defined accurately. Under the transformation given in (2.5)

$$\frac{\partial \psi}{\partial x} = \frac{\partial \psi}{\partial \zeta} - \frac{\eta f'}{f} \frac{\partial \psi}{\partial \eta},$$

(2.6)

$$\frac{\partial \psi}{\partial y} = \frac{1}{f} \frac{\partial \psi}{\partial \eta},$$

(2.7)

$$\frac{\partial^2 \psi}{\partial x^2} = \frac{\partial^2 \psi}{\partial \zeta^2} + 2\eta \left(\frac{f'}{f}\right)^2 \frac{\partial \psi}{\partial \eta} + \left(\frac{\eta f'}{f}\right)^2 \frac{\partial^2 \psi}{\partial \eta^2} - 2\eta \left(\frac{f'}{f}\right) \frac{\partial^2 \psi}{\partial \zeta \partial \eta},$$

(2.8)

$$\frac{\partial^2 \psi}{\partial y^2} = \frac{1}{f^2} \frac{\partial^2 \psi}{\partial \eta^2}. \tag{2.9}$$

All ω derivatives have the same transformation as ψ. The governing equations (2.1) to (2.3) become

$$\omega = -\left[\frac{\partial^2 \psi}{\partial \zeta^2} + 2\eta \left(\frac{f'}{f}\right)^2 \frac{\partial \psi}{\partial \eta} + \frac{\left\{1 + (f'\eta)^2\right\}}{f^2} \frac{\partial^2 \psi}{\partial \eta^2} - 2\eta \frac{f'}{f} \frac{\partial^2 \psi}{\partial \zeta \partial \eta}\right], \tag{2.10}$$

$$\frac{\partial \omega}{\partial t} + \frac{\partial(u\omega)}{\partial \zeta} - \frac{\eta f'}{f} \frac{\partial(u\omega)}{\partial \eta} + \frac{1}{f} \frac{\partial(v\omega)}{\partial \eta} = \frac{1}{Re}\left[\frac{\partial^2 \omega}{\partial \zeta^2} + 2\eta \left(\frac{f'}{f}\right)^2 \frac{\partial \omega}{\partial \eta} + \right.$$

$$\left. \frac{\left\{1 + (f'\eta)^2\right\}}{f^2} \frac{\partial^2 \omega}{\partial \eta^2} - 2\eta \frac{f'}{f} \frac{\partial^2 \omega}{\partial \zeta \partial \eta}\right], \tag{2.11}$$

$$u = \frac{1}{f} \frac{\partial \psi}{\partial \eta} \quad \text{and} \quad v = -\frac{\partial \psi}{\partial \zeta} + \frac{\eta f'}{f} \frac{\partial \psi}{\partial \eta}. \tag{2.12}$$

2.4   Discretization

NW	N	NE
W	P	E
SW	S	SE

The central difference discretization [7] yields the following,

$$\left(\frac{\partial \psi}{\partial \zeta}\right)_P = \frac{(\psi_E - \psi_W)}{2\Delta\zeta},$$

$$\left(\frac{\partial \psi}{\partial \eta}\right)_P = \frac{(\psi_N - \psi_S)}{2\Delta\eta},$$

$$\left(\frac{\partial^2 \psi}{\partial \zeta^2}\right)_P = \frac{(\psi_E - 2\psi_P + \psi_W)}{2\Delta\zeta^2},$$

$$\left(\frac{\partial^2 \psi}{\partial \eta^2}\right)_P = \frac{(\psi_N - 2\psi_P + \psi_S)}{2\Delta\eta^2},$$

$$\left(\frac{\partial^2 \psi}{\partial \zeta \partial \eta}\right)_P = \frac{(\psi_{NE} - \psi_{SE} - \psi_{NW} + \psi_{SW})}{4\Delta\zeta\Delta\eta},$$

$$\left(\frac{\partial \omega}{\partial t}\right)_P = \frac{(\omega_P - \omega_{old})}{\Delta t}.$$

Forward difference discretization is used for the transient term, and central difference for the rest of the terms. If the velocity at a point is negative, the information will be carried in the backward direction; at that point backward difference has been used for the convective terms. Similarly if the velocity at a point is positive, the information will be carried in the forward direction; at that point forward difference has been used for the convective terms, i.e. upwinding is done.

From (2.10) the discretized equation for the streamfunction becomes

$$A_P\psi_P = \psi_E A_E + \psi_W A_W + \psi_N A_N + \psi_S A_S + \psi_{NE} A_{NE} + \psi_{SE} A_{SE} +$$

$$\psi_{NW} A_{NW} + \psi_{SW} A_{SW} + \omega_P. \tag{2.13}$$

where

$$A_P = \left[\frac{2}{(\Delta\zeta)^2} + \frac{2\left(1 + (f'\eta)^2\right)}{f^2(\Delta\eta)^2}\right],$$

$$A_E = \frac{1}{(\Delta\zeta)^2},$$

$$A_W = A_E,$$

$$A_N = \left[\frac{\left\{1 + (f'\eta)^2\right\}}{f^2(\Delta\eta)^2} + \frac{\eta}{\Delta\eta}\left(\frac{f'}{f}\right)^2\right],$$

$$A_S = A_N,$$

$$A_{NE} = \left[\frac{-\eta}{2\Delta\zeta\Delta\eta}\left(\frac{f'}{f}\right)\right],$$

$$A_{SE} = A_{NE},$$

$$A_{NW} = -A_{NE},$$

$$\text{and}\quad A_{SW} = -A_{NE}.$$

Applying the above finite difference for the convective and viscous term and using a forward time-march for the transient term, (2.11) yields the following discrete equations for ω

$$\omega_P = \omega_{old} + \Delta t\left[-\frac{\partial(u\omega)}{\partial\zeta} + \frac{\eta f'}{f}\frac{\partial(u\omega)}{\partial\eta} - \frac{1}{f}\frac{\partial(v\omega)}{\partial\eta} + \frac{1}{Re}\frac{\partial^2\omega}{\partial\zeta^2} - \frac{1}{Re}2\eta\left(\frac{f'}{f}\right)\frac{\partial^2\omega}{\partial\zeta\partial\eta} + \right.$$
$$\left.\frac{1}{Re}2\eta\left(\frac{f'}{f}\right)^2\frac{\partial\omega}{\partial\eta} + \frac{1}{Re}\frac{\left\{1 + (\eta f'')^2\right\}}{f^2}\right]. \tag{2.14}$$

2.5 Boundary Conditions

There are three types of boundary conditions needed for this problem [7,8]. The first is the exit boundary condition. The straight section following the divergent section is taken to be long enough so that the flow near the right of the computational domain is independent of ζ. In other words $\partial/\partial\zeta = 0$ for all the relevant flow parameters. For a separated flow, a much longer computational domain needs to be employed so that this condition can be used at the exit.

Symmetry boundary conditions are created by creating fictitious points just outside the flow domain. These fictitious points mirror the fluid properties just inside the flow domain. Thus at the symmetry boundary, i.e. at the centerline, the relationship for the streamfunction is $\psi_{i+1} = \psi_{i-1}$ at point i. This is equivalent to the 2 point second derivative at i being equal to zero.

The third boundary condition concerns vorticity at the walls. At a solid boundary the update expression for ω is,

$$\omega_p = \frac{(1 + f'^2)}{f^2}\frac{2(\psi_p - \psi_i)}{(\Delta\eta)^2}, \quad y = \pm 1$$

where Δ and i are in the direction (inward) normal to the surface. The boundary conditions at the entry ($\zeta = 0$) are

$$u = 1 - \eta^2,$$

$$v = 0,$$

$$\psi = \eta - \frac{\eta^3}{3},$$

$$\omega = 2\eta,$$

No slip condition at the wall :

$$\frac{\partial \psi}{\partial \zeta} = 0, \quad \frac{\partial \psi}{\partial \eta} = 0.$$

Exit condition :

$$\partial / \partial \zeta = 0,$$

Boundary condition at centerline :

Symmetry boundary condition at the centerline is applied by creating fictitious points just outside the flow domain as described above.

2.6   Solution Method

The solution method [5] consists of the following steps:

i) Setting of initial and boundary conditions for the flow parameters.

ii) Calculation of the vorticity at the new time step from the dynamic vorticity equation. Any standard time marching method may be used for this purpose.

iii) Having the vorticity at the new time step, the next step is to compute streamfunction. This is the most time-consuming part in the program. Any iterative scheme may be used for this part. But multigrid technique is probably the fastest method to solve this. Multigrid technique has been used for

the present work. This technique has been elaborated in Chapter 4.

iv) Finally, having the streamfunction, the velocity components are computed.

v) For a steady state problem these steps are repeated till the vorticity residual reduces to a value below a prescribed limit.

Chapter 3

Flow in an Axisymmetric Pipe

3.1 Summary

In a similar manner as for the convergent-divergent channel a code was developed for two dimensional, incompressible flow in a convergent-divergent axisymmetric pipe. The vorticity and streamfunction approach has been used in this case too. To accelerate the rate of convergence, multigrid technique has been implemented. This technique has been elaborated in Chapter 4. This code can be used for both steady state and transient problem. The method of solution is the same as explained in the Chapter 2.

3.2 Governing Equations

$$\frac{\partial \omega}{\partial t} + u\frac{\partial \omega}{\partial r} + v\frac{\partial \omega}{\partial x} = \frac{\omega u}{r} + \frac{1}{Re}\left[\frac{\partial}{\partial r}\left(\frac{1}{r}\frac{\partial(r\omega)}{\partial r}\right)\right] + \frac{1}{Re}\frac{\partial^2 \omega}{\partial x^2}, \qquad (3.1)$$

$$\omega = -\frac{1}{r}\frac{\partial^2 \psi}{\partial r^2} + \frac{1}{r^2}\frac{\partial \psi}{\partial r} - \frac{1}{r}\frac{\partial^2 \psi}{\partial x^2}, \qquad (3.2)$$

17

$$u = \frac{1}{r}\frac{\partial \psi}{\partial r}, \quad v = -\frac{1}{r}\frac{\partial \psi}{\partial x}, \qquad \qquad (3.3)$$

where the axial and radial coordinates are (x, r), and the corresponding velocity components are (u, v).

Equations (3.1) to (3.3) are non-dimensional equations with all non-dimensionalized as follows:

$$u = \frac{u_d}{U}, \quad v = \frac{v_d}{U}, \quad x = \frac{x_d}{L}, \quad y = \frac{y_d}{L}, \quad \omega = \frac{\omega_d}{\omega_0}, \quad \psi = \frac{\psi_d}{\psi_0}$$

$$(3.4)$$

where U is the velocity at the centerline in the inlet. L is the half channel width at the entry, ψ_0 and ω_0 is the value of the streamfunction and vorticity respectively at the wall in the inlet section. The 'd' stands for dimensional quantity.

3.3 Transformation of coordinate system

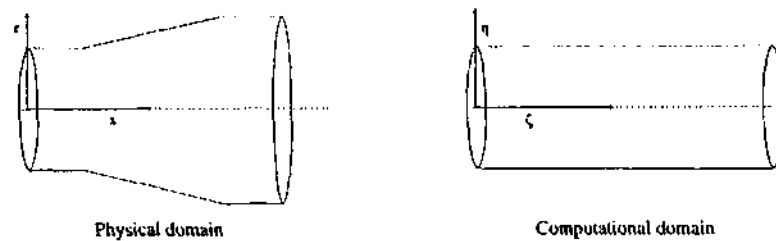Physical domain   Computational domain

Figure 3.1: Schematic diagram of axisymmetric pipe

Fig.(3.1) is not to scale, in the geometry we have considered, the divergent part is much shorter than the straight exit part. A long straight section is provided to enable the exit flow to be defined accurately.

The use of a finite difference method to solve the flow in this geometry is facilitated by a transformation of coordinates. The transformation from the physical domain to the computational domain is given by the following equations.

$$x = \zeta,$$

$$r = \eta f(x), \tag{3.5}$$

where $f(x)$ is a function representing the shape of the wall.

The above transformation [2], yields expressions similar in form to (2.6) to (2.9) with y replaced by r. Under the transformation given in (3.5), equations from (3.1) to (3.3) become,

$$\frac{\partial \omega}{\partial t} + \frac{u}{f}\frac{\partial \omega}{\partial \eta} + v\frac{\partial \omega}{\partial \zeta} - \frac{\eta f' v}{f}\frac{\partial \omega}{\partial \eta} = \frac{u\omega}{\eta f} + \frac{1}{Re}\left[\frac{\partial^2 \omega}{\partial \zeta^2} - 2\eta\left(\frac{f'}{f}\right)\frac{\partial^2 \omega}{\partial \zeta \partial \eta} + \right.$$

$$\left. \left\{\frac{1}{f^2} + \eta^2\left(\frac{f'}{f}\right)^2\right\}\frac{\partial^2 \omega}{\partial \eta^2} + \left\{\frac{1}{\eta f^2} + 2\eta\left(\frac{f'}{f}\right)^2\right\}\frac{\partial \omega}{\partial \eta} - \frac{\omega}{\eta^2 f^2}\right], \tag{3.6}$$

$$\frac{\partial^2 \psi}{\partial \zeta^2} - 2\eta\left(\frac{f'}{f}\right)\frac{\partial^2 \psi}{\partial \zeta \partial \eta} + \left[\frac{1}{f^2} + \eta^2\left(\frac{f'}{f}\right)^2\right]\frac{\partial^2 \psi}{\partial \eta^2} + \left[2\eta\left(\frac{f'}{f}\right)^2 - \frac{1}{\eta f^2}\right]\frac{\partial \psi}{\partial \eta} = -\eta f \omega, \tag{3.7}$$

$$u = \frac{1}{\eta f^2}\frac{\partial \psi}{\partial \eta}, \quad v = -\frac{1}{\eta f}\left[\frac{\partial \psi}{\partial \zeta} - \frac{\eta f'}{f}\frac{\partial \psi}{\partial \eta}\right]. \tag{3.8}$$

3.4   Discretization

The discretization used in this case is the same as that explained in sect.(2.4). Applying the discretization in (3.7) and solving for ψ at the point p, yields the following discretized equation,

$$\psi_P A_P = \psi_E A_E + \psi_W A_W + \psi_N A_N + \psi_S A_S + \psi_{NE} A_{NE} + \psi_{SE} A_{SE} +$$

$$\psi_{NW} A_{NW} + \psi_{SW} A_{SW} + \omega_P A_\omega, \tag{3.9}$$

where

$$A_P = \left[\frac{2}{(\Delta\zeta)^2} + \frac{2\left(1 + (f'\eta)^2\right)}{f^2(\Delta\eta)^2} \right],$$

$$A_E = \left[\frac{1}{(\Delta\zeta)^2} \right],$$

$$A_W = A_E,$$

$$A_N = \left[\left\{ 2\eta\left(\frac{f'}{f}\right)^2 - \frac{1}{\eta f^2} \right\} \frac{1}{2\Delta\eta} + \frac{\left\{ 1 + (\eta f')^2 \right\}}{f^2} \frac{1}{\Delta\eta^2} \right],$$

$$A_S = \left[-\left\{ 2\eta\left(\frac{f'}{f}\right)^2 - \frac{1}{\eta f^2} \right\} \frac{1}{2\Delta\eta} + \frac{\left\{ 1 + (\eta f')^2 \right\}}{f^2} \frac{1}{\Delta\eta^2} \right],$$

$$A_{NE} = \left[\frac{-\eta f'}{2f\Delta\zeta\Delta\eta} \right],$$

$$A_{SE} = -A_{NE},$$

$$A_{NW} = -A_{NE},$$

$$A_{SW} = A_{NE},$$

and $A_\omega = \eta f$.

Similarly, from (3.6)

$$\omega_p = \omega_{old} + \Delta t \left[-\frac{u}{\eta f} \frac{\partial \omega}{\partial \eta} - \frac{v}{\eta} \frac{\partial \omega}{\partial \zeta} + \frac{f'v}{f} \frac{\partial \omega}{\partial \eta} + \frac{u\omega}{\eta^2 f} + \frac{1}{Re} \frac{\partial^2 \omega}{\partial \zeta^2} - 2\eta \left(\frac{f'}{f} \right) \frac{1}{Re} \frac{\partial^2 \omega}{\partial \zeta \partial \eta} + \right.$$

$$\left. \frac{[1 + (\eta f')^2]}{f^2} \frac{1}{Re} \frac{\partial^2 \omega}{\partial \eta^2} + \frac{[1 + 2\eta^2 f'^2]}{\eta f^2} \frac{1}{Re} \frac{\partial \omega}{\partial \eta} - \frac{\omega}{\eta^2 f^2} \frac{1}{Re} \right] \qquad (3.10)$$

3.5   Solution Method

The solution method and the boundary conditions for this case are the same as flow in a divergent channel described in (2.6). But in the case of axisymmetric flow, there could be singularities in the equations at $r = 0$ $(\eta = 0)$. So equations (3.10) and (3.8) are multiplied by η throughout, and we solve for $u\eta$, $v\eta$, ψ, ω using the multigrid technique.

Chapter 4

Multigrid Method

4.1 Introduction

The multigrid method provides algorithms which can be used to accelerate the rate of convergence of iterative methods, such as Jacobi or Gauss-Seidel, for solving elliptic partial differential equations [9–11]. Iterative methods start with an approximate guess for the solution to the differential equation. In each iteration, the difference between the approximate solution and the exact solution is made smaller. One can break up this difference or error into components of different wavelength, for example by using Fourier analysis. In general the error will have components of many different wavelengths i.e., there will be short and long wavelength error components. Algorithms like Jacobi or Gauss-Seidel are local because the new value for the solution at any lattice site depends only on the value of the previous iterate at neighboring points. Such local algorithms are generally more efficient in reducing

22

short wavelength error components. The basic idea behind multigrid methods is to reduce long wavelength error components by updating blocks of grid points.

4.2   Multigrid solution of Poisson's equation in 2-D

Poisson's equation in 2-D is

$$\frac{\partial^2 u}{\partial x^2} + \frac{\partial^2 u}{\partial y^2} = -f(x,y) \tag{4.1}$$

where the unknown solution $u(x,y)$ is determined by the given source term $f(x,y)$ in a closed region. Let's consider a square domain $0 \le x, y \le L$ with homogeneous Dirichlet boundary conditions $u = 0$ on the perimeter of the square. The equation is discretized on a grid with N+2 lattice points, i.e, N interior points and two boundary points, in the x and y directions. At any interior point, the exact solution obeys

$$u_{i,j} = \left[u_{i+1,j} + u_{i-1,j} + u_{i,j+1} + u_{i,j-1} + h^2 f_{i,j} \right]. \tag{4.2}$$

The number of different grids employed is called the number of multigrid levels l. The number of interior lattice points in the x and y directions is then taken to be 2^l, so that $N = 2^l + 2$, and the lattice spacing $h = 1/(N - 1)$. N is chosen in this manner so that the downward multigrid iteration can

construct a sequence of coarser lattices with

$$2^{l-1} \rightarrow 2^{l-2} \rightarrow \ \dots\dots \rightarrow 2^0 = 1 \qquad (4.3)$$

interior points in the x and y directions.

Suppose that $u(x, y)$ is the approximate solution at any stage in the calculation, and $u_{exact}(x, y)$ is the solution which we are trying to find. The multigrid algorithm uses the following definitions:

The correction

$$v = u_{exact} - u \qquad (4.4)$$

is the function which must be added to the approximate solution to give the exact solution. **The residual or defect** is defined as

$$r = \nabla^2 u + f. \qquad (4.5)$$

From the above expressions, it is clear that the correction and residual are related by the following equation

$$\nabla^2 v = \left[\nabla^2 u_{exact} + f \right] - \left[\nabla^2 u + f \right] = -r. \qquad (4.6)$$

This equation has exactly the same form as Poisson's equation with v playing the role of the unknown function and r playing the role of the known source function.

4.3   Simple V-cycle algorithm

The simplest multigrid algorithm is based on a two-grid improvement scheme.
Considering two grids:

- a fine grid with $N = 2^l + 2$ points in each direction, and

- a coarse grid with $N = 2^{l-1} + 2$ points.

It is needed to relate one grid to another, i.e., given any function on the
lattice, it is needed to

- restrict the function from fine $\rightarrow$ coarse, and

- prolongate or interpolate the function from coarse $\rightarrow$ fine.

Figure 4.1: Simple V-cycle in full-multigrid algorithm

4.4   Multigrid algorithm

The multigrid algorithm follows the following steps:

1. If $l = 0$ there is only one interior point, so solve exactly for

$$u_{1,1} = \Big(u_{0,1} + u_{2,1} + u_{1,0} + u_{1,2} + h^2 f_{1,1}\Big)/4.$$

2. Otherwise, calculate the current $N = 2^l + 2$.

3. Perform a few pre-smoothing iterations using a local algorithm such as Gauss-Seidel. The idea is to damp or reduce the short wavelength errors in the solution.

4. Estimate the correction $v = u_{exact} - u$ as follows:

- Compute the residual

$$r_{i,j} = \frac{1}{h^2}\Big[u_{i+1,j} + u_{i-1,j} + u_{i,j+1} + u_{i,j-1} - 4u_{i,j}\Big] + f_{i,j}.$$

- Restrict the residual $r \to R$ to the coarser grid.

- Set the coarser grid correction $V = 0$ and improve it recursively.

- Prolongate the correction $V \to v$ onto the finer grid.

5. Correct $u \to u + v$.

6. Perform a few post-smoothing Gauss-Seidel iterations and return the improved u to the next finer grid.

In this thesis, unless otherwise specified a six-level multigrid algorithm was used, with the finest grid being 128x128, with V-cycle as shown in fig.(4.1).

Chapter 5

Validation of the present code

5.1 Test case 1: Developing flow in a channel

Two test cases were run to validate the present code against bench-mark results. The first test case is a developing laminar channel flow [12]. This case with a uniform inflow with velocity U at the entrance on the left in fig.(5.1) developed rapidly into a fully developed flow with an unchanging velocity profile.

L = 1.0

S = 40.0
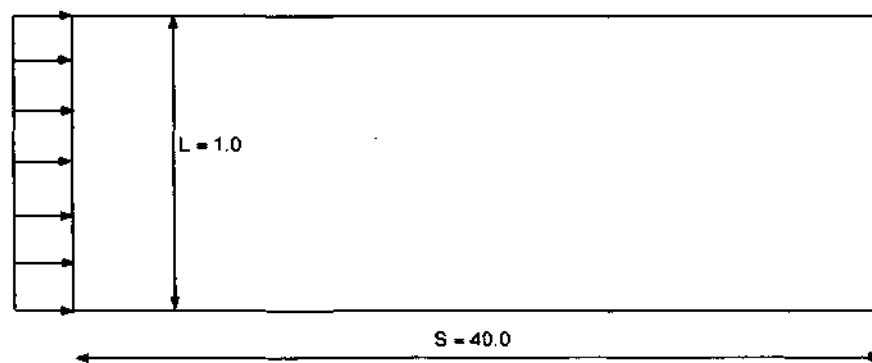
Figure 5.1: Test case of developing channel flow.

27

This test case has the following features: Incompressible, laminar, steady flow with constant fluid properties. $Re_L = 75$, where L is width of channel.

The velocity profiles at a distance of $x = 1$ and $x = 4$ are seen from the following fig.(5.2) to compare very well with the bench-mark computational results of Mc.Donald $et\ al.$ and Dogrouz [12]. It is to be noted that in the present computations with 64x64 number of points, the residue of vorticity falls to 10^{-10}, while in Dogrouz's computation, the grid is 45x45, and computation is stopped when the residue falls to 10^{-4}. Incidentally, he used the Navier-Stokes equations as the governing equations.
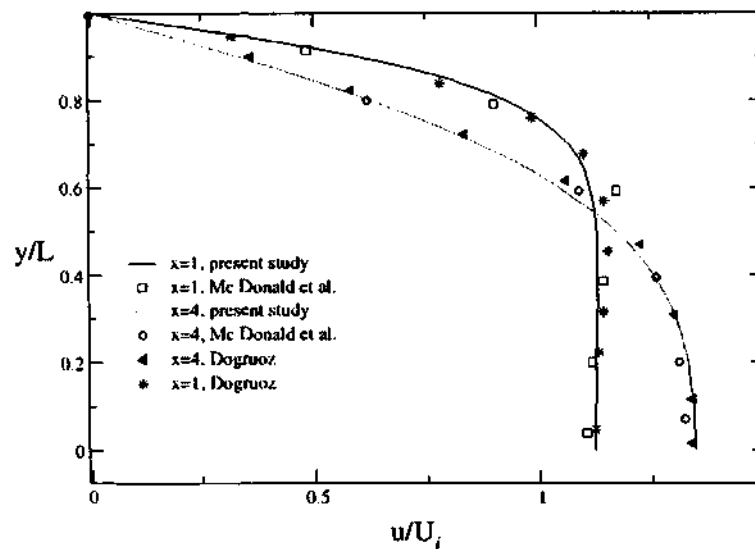
Figure 5.2: Comparison of velocity profiles from the present code with bench mark computational results.

Another check has been made for the entry flow in a channel. The test case consists of a channel, with uniform inlet flow and long enough to give a
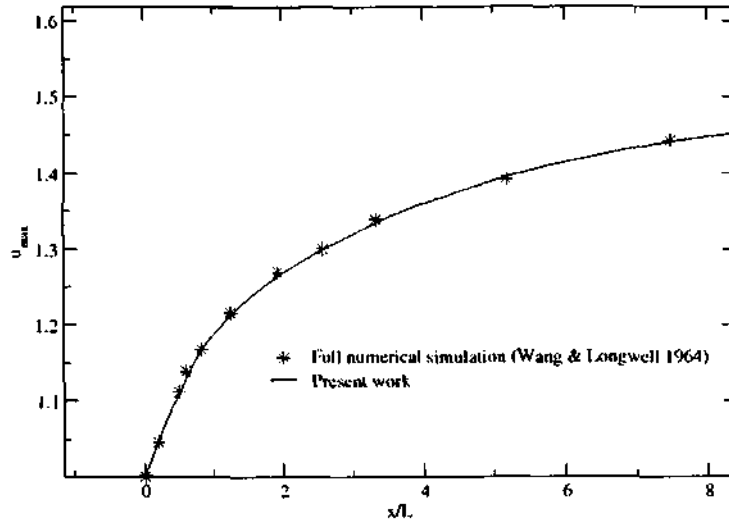
Figure 5.3: Velocity at the centerline Vs distance from the entry, Re=75.

fully developed flow with an unchanging velocity profile at the outlet. The
downstream development of the centerline velocity, obtained from the present
code has been compared in fig.(5.3) to those of Wang and Longwell (1964)
presented in [13]. The comparison is again good. The convergence behaviour
of the code for the above developing flow in a channel is shown in fig.(5.4).
Here, ω_{rsd} is the departure from steady state in the vorticity across the
domain. It is defined as the sum over the domain of the absolute value of
the difference in the local ω between consecutive time steps, i.e,

$$\text{omegarsd} \equiv \sum_{i=1}^{n}\sum_{j=1}^{n} \mid \omega_{i,j}^{\tau} - \omega_{i,j}^{\tau-1} \mid$$

Other results for the above test case, namely streamwise and normal velocity
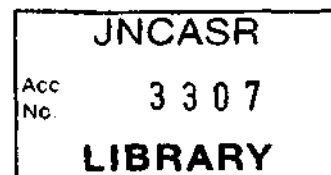
profiles and streamfunction profiles at different locations in the downstream of the channel are shown in fig.(5.5) to fig.(5.7). It can be seen in fig.(5.5) that at $x = 40$ the maximum streamwise velocity is 1.5, i.e, the flow is fully developed at $x = 40$. Computations with $x > 40$ have been conducted to ensure the validity of the outlet conditions. It has been found that the velocity profile is already parabolic at $x = 40$ even though domain is larger.
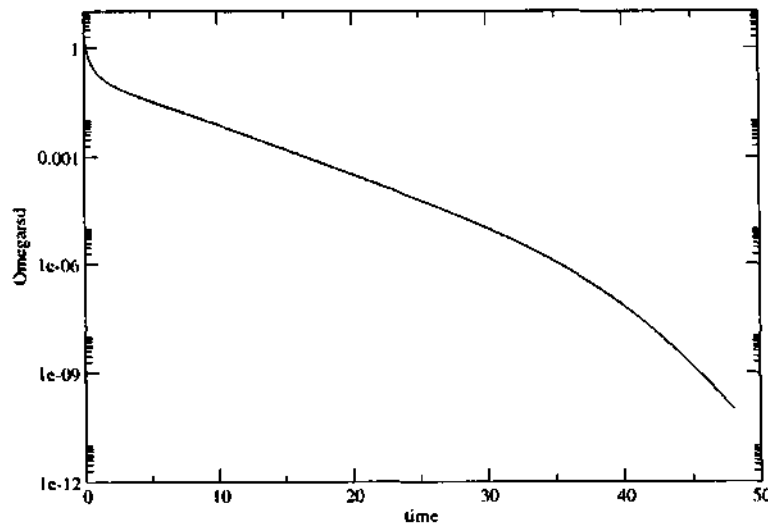
Figure 5.4: ω_{rsd} Vs time, Re = 75, Domain = 1:40.
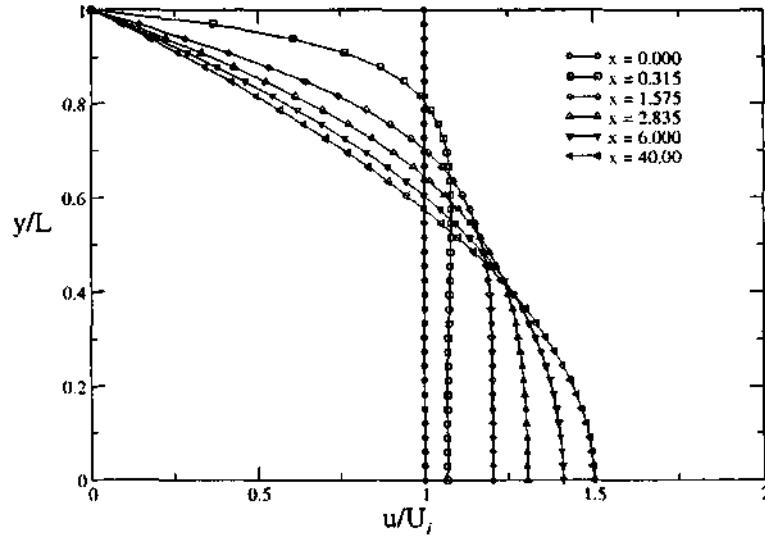
Figure 5.5: Streamwise velocity profile, Re = 75, Domain = 1:40.
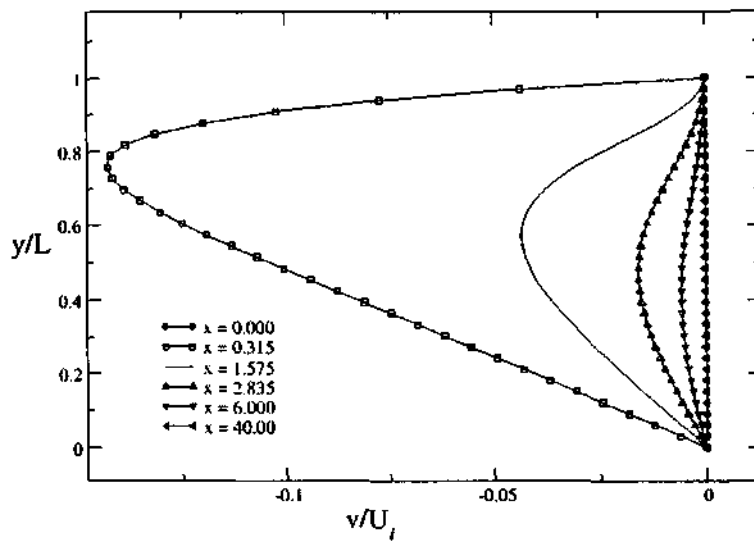
Figure 5.6: Normal velocity profile, Re = 75, Domain = 1:40.
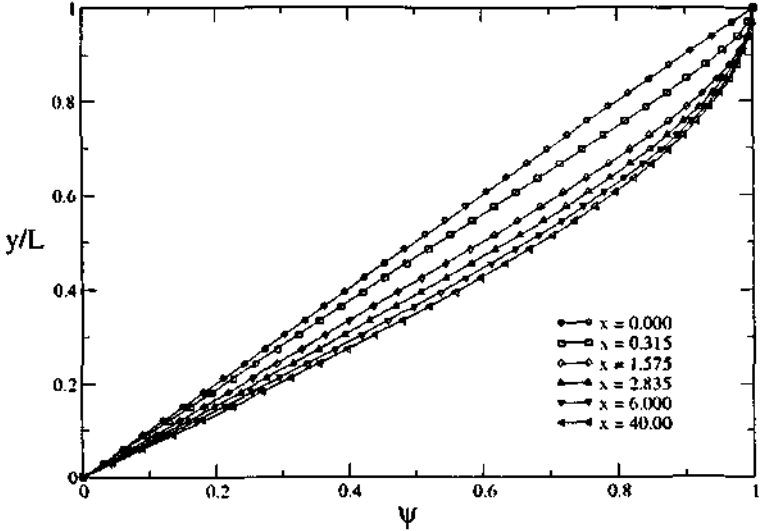
Figure 5.7: Streamfunction profile, Re = 75, Domain = 1:40.

5.2 Test case 2: Flow in a backward-facing step

In the following test case the present result has been validated by the experimental measurements of flow near a backward-facing step by Armaly *et al.* [14]. In the present test case the physical situation consists of a backward-facing step with $D/d = 2$ as shown in fig.(5.8). The inlet is a parabolic profile and the exit boundary condition ($\partial/\partial x = 0$) has been applied far downstream (at x=33d), where the profile has been checked to be unchanging in x. For the computation 34x66 number of grids has been used. The present velocity profiles match very well at different streamwise locations, an example of which is shown in fig.(5.9).
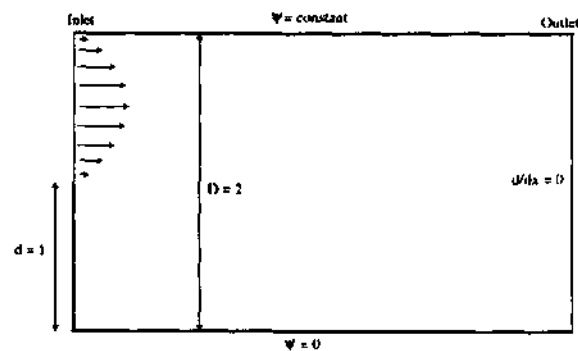
Figure 5.8: Geometry of the test case, as given by Armaly *et al.* (1983) and prescribed here.
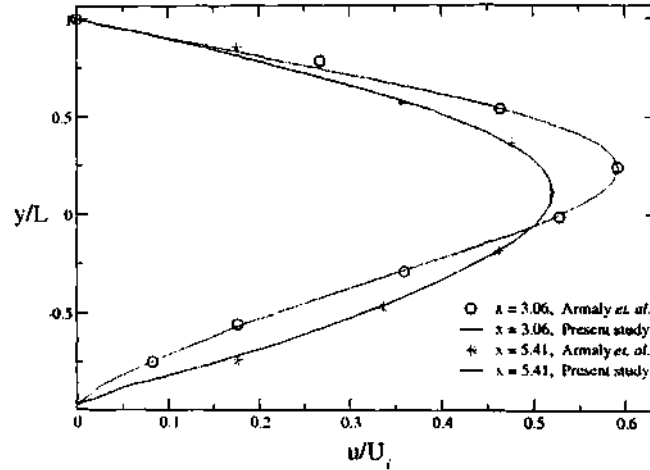
Figure 5.9: Comparison of the present results with Armaly *et al.* at two different downstream locations, based on Re = 75.

In the fig.(5.10), the oscillating behaviour of ω_{rsd} can be seen. By the present method, it is not found possible to decrease the ω_{rsd} to below 10^{-4} using the prescribed number of grids. This is because the solution begins to alternate between two states. It has been considered here as sufficiently close to a steady state. The streamlines and velocity profiles for the above flow are shown in fig.(5.11) to fig.(5.14). It is clear from the fig.(5.12) that the streamwise velocity profile developed to an unchanging profile at $x =$ 33.15. The corresponding normal velocity and streamfunction profiles are also shown in fig.(5.13) and fig.(5.14) respectively. The separation bubble in this flow is clearly visible in all the figures.
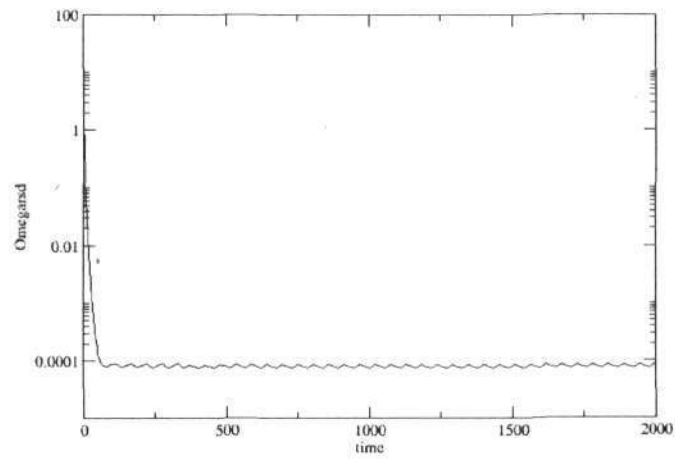
Figure 5.10: ω_{rsd} Vs time, Re $= 75$.
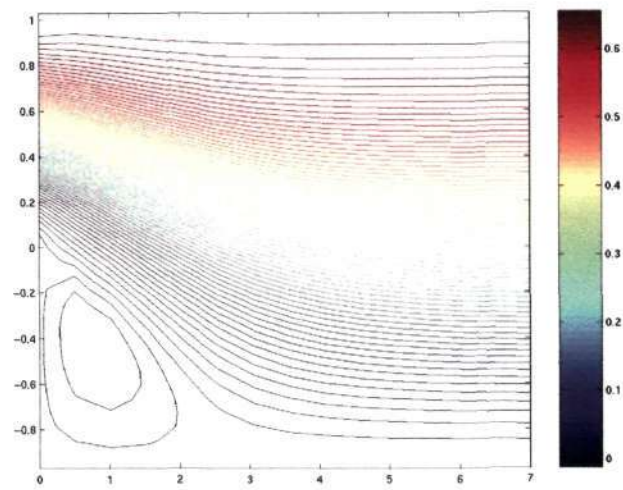
Figure 5.11: Streamlines at the steady state, Re $= 75$.
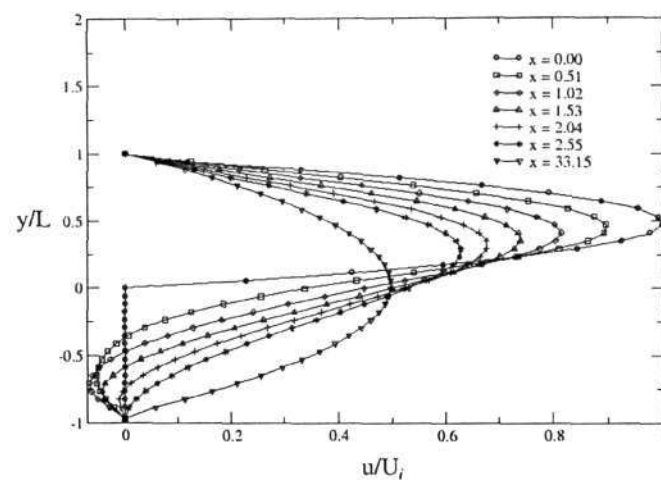
Figure 5.12: Streamwise velocity profile, Re = 75.
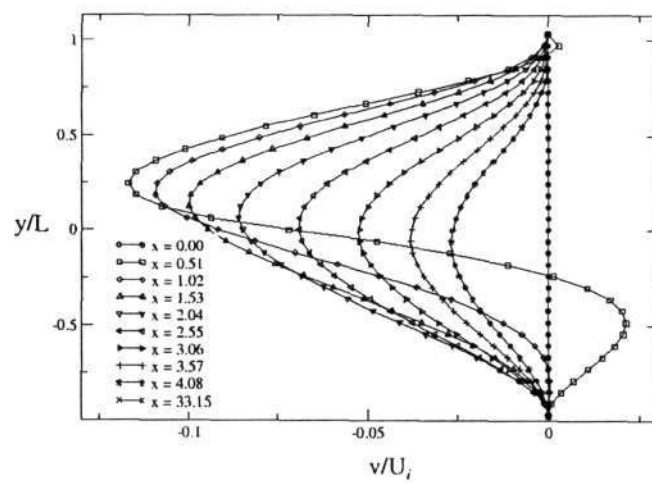
Figure 5.13: Normal velocity profile, Re = 75.
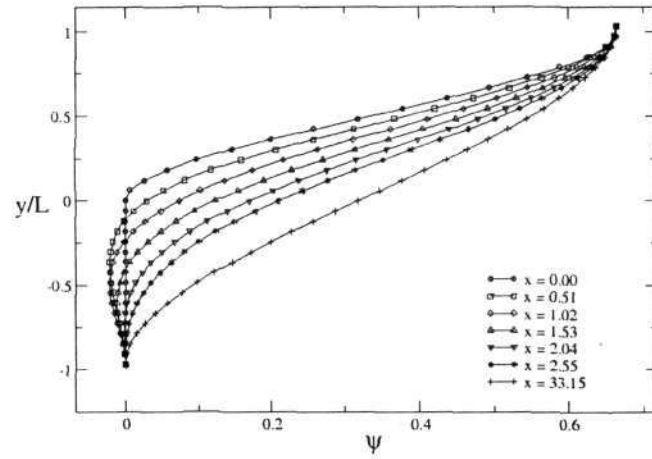
Figure 5.14: Streamfunction profile, Re = 75.

5.3   Comparison of the full-multigrid with Gauss-Seidel technique

For the comparison of the full-multigrid with Gauss-Seidel method, the heat conduction equation has been solved by both the techniques for the following physical system. This system consists of a slab, whose top wall has been maintained at a non-dimensional temperature 1 and all other walls are at zero, as shown in fig.(5.15).

Governing equation for this test case:

$$\frac{\partial^2 t}{\partial x^2} + \frac{\partial^2 t}{\partial y^2} = q, \tag{5.1}$$

t = 1

t = 0   t = 0

t = 0
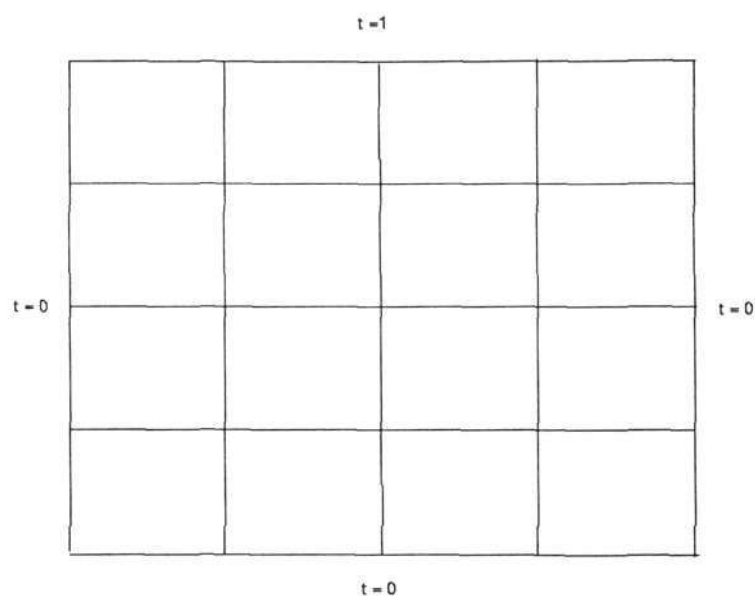
Figure 5.15: test case for multigrid technique.

where q is heat source. It has been taken to be 1 through out the domain for the present case. The discretized equation for Gauss-Seidel is of the following form.

$$A_P t_P{}^{r+1} = A_E t_E{}^r + A_W t_W{}^r + A_N t_N{}^r + A_S t_S{}^r - q. \tag{5.2}$$

A six level multigrid algorithm, with 128x128 grid points has been used for this case.
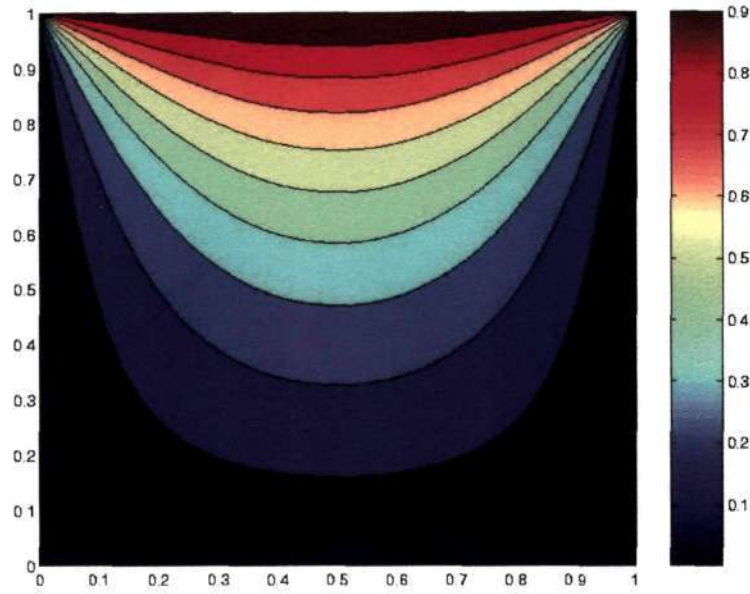
Figure 5.16: Temperature profile for the test case.
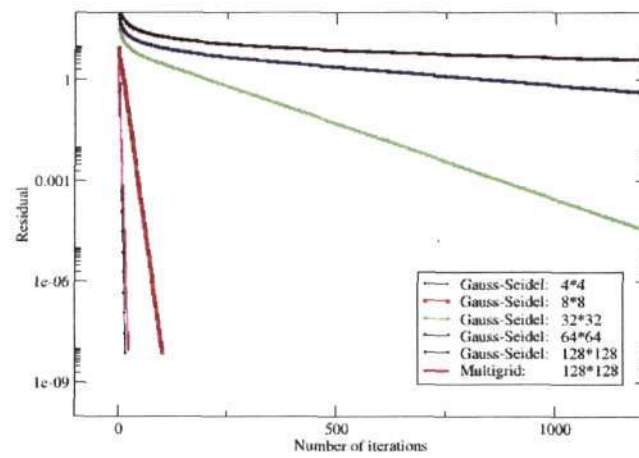
Figure 5.17: Comparison of multigrid with Gauss-Seidel technique.

It is clear from the fig.(5.17), the solution of 128x128 grids, with full-multigrid algorithm is converging as fast as a solution of 4x4 grids in Gauss-Seidel method. For simulation of the separated flow, a large number of grid points are required in the separated region. Therefore multigrid algorithm is found to be very useful in this case.

Chapter 6

Results and Discussions

6.1 Results: Flow in a divergent channel

The geometry for the present computation, of the flow in a divergent channel has been shown in fig.(6.1). As already explained, in spatially de-
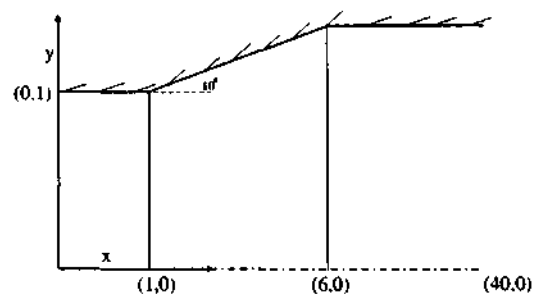
Figure 6.1: Physical domain for the flow in a divergent channel. Figure is not to scale.

veloping flows, especially those where a region of flow separation exists, the

exit boundary condition needs special care. In the present case, the exit boundary condition is applied far downstream in a location where the flow has unchanging velocity profile.

The convergence behaviours of the vorticity residual for different Reynolds numbers are shown in fig.(6.2) and fig.(6.3). As it can be seen in fig.(6.2), the vorticity residual goes down steadily to below a value of 10^{-9}. The variations of streamwise velocity profiles at different locations in the downstream for $Re = 100$, and angle of divergence $= 10^0$ are shown in fig.(6.4). The flow is separated at $x = 5.89$ and again reattaches at $x \sim 10$, giving unchanged parabolic profiles after 36.8. The corresponding normal velocity and stream-function profiles are shown in fig.(6.5) and fig.(6.4). The vorticity profile for this case is shown in fig.(6.6). Computations with a longer domain are being performed to ensure that the exit boundary conditions is applied at a safe x location in the downstream.
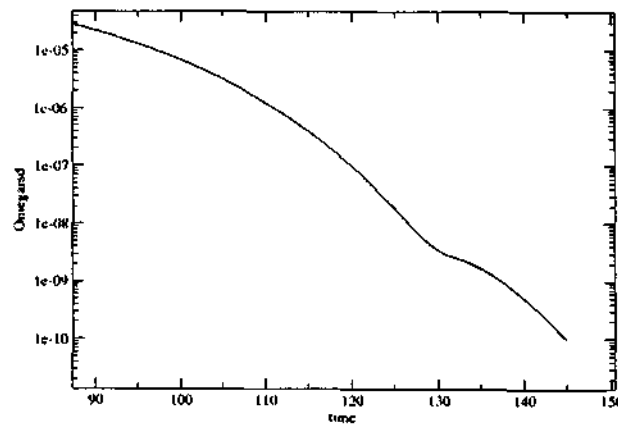
Figure 6.2: ω_{rsd} Vs time, $Re = 100$ and angle of divergence $= 10^0$.
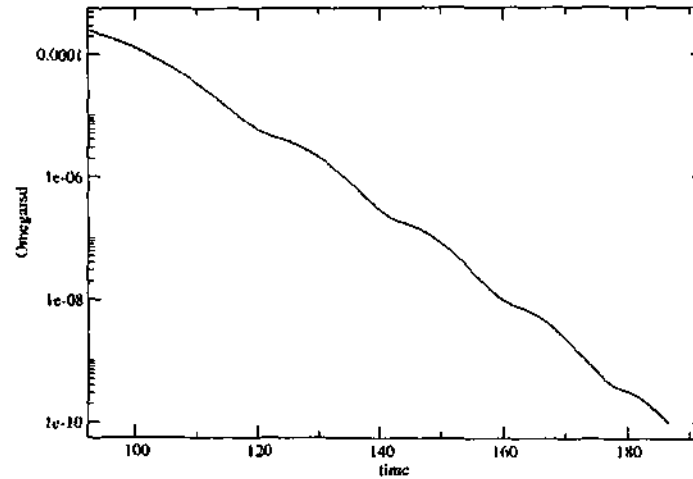
Figure 6.3: ω_{rsd} Vs time, $Re = 200$ and angle of divergence $= 10^0$.

As already explained in chapter 1, Eagles [1] used a similarity profile in the stability calculation, although his geometry is different from the present case, to get a rough idea about the effect of Reynolds number and angle of divergence in the stability calculation, the present profile has been compared with the Eagles profile in fig.(6.8) and fig.(6.9). It was found that for small Reynolds number and angle of divergence it is reasonable to use the similarity profile but even for moderate angles of divergence, such as 5^0 [fig.(6.9)] the analytical profile needs to be modified.
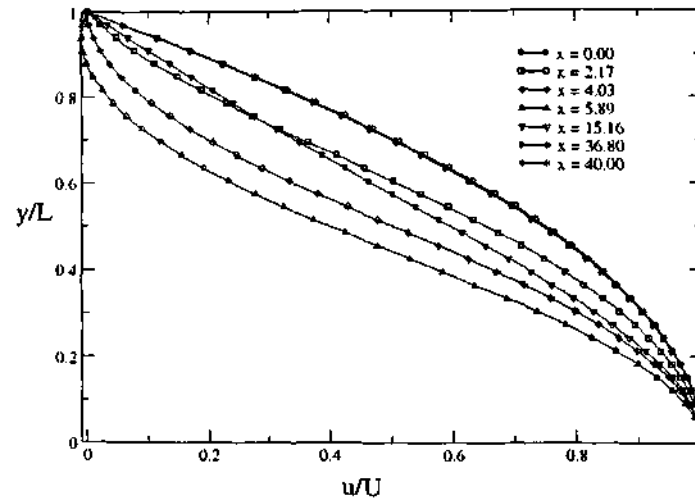
Figure 6.4: Streamwise velocity profile, $Re = 100$ and angle of divergence $= 10^0$.
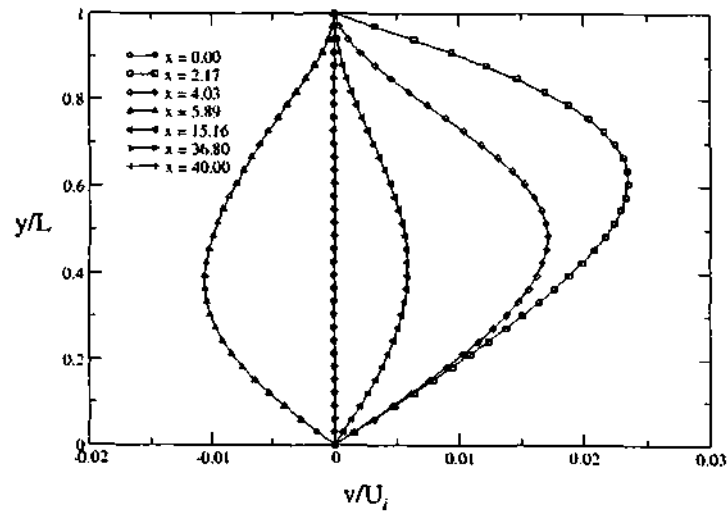
Figure 6.5: Normal velocity profile, $Re = 100$ and angle of divergence $= 10^0$.
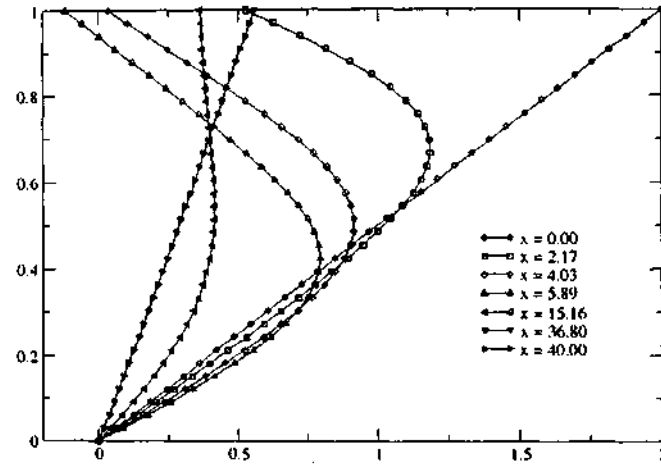
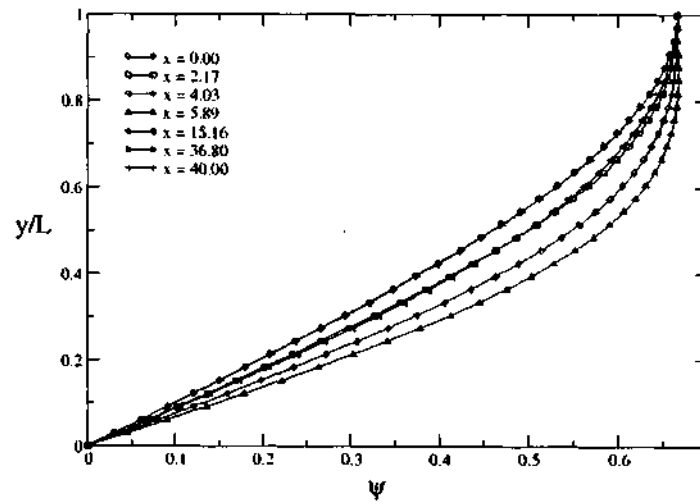Figure 6.6: Vorticity profile at steady state, $Re = 100$ and angle of divergence $= 10^0$.

Figure 6.7: Streamfunction at steady state, $Re = 100$ and angle of divergence$= 10^0$.

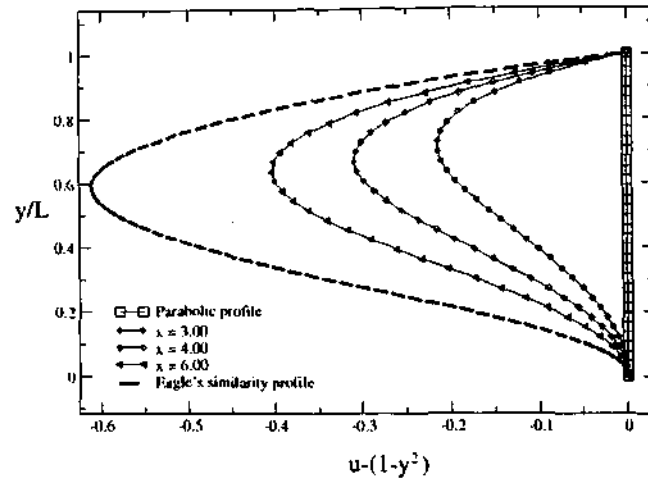Figure 6.8: Comparison of Eagle's similarity profile with the present result, $Re = 100$ and angle of divergence $= 10^0$.
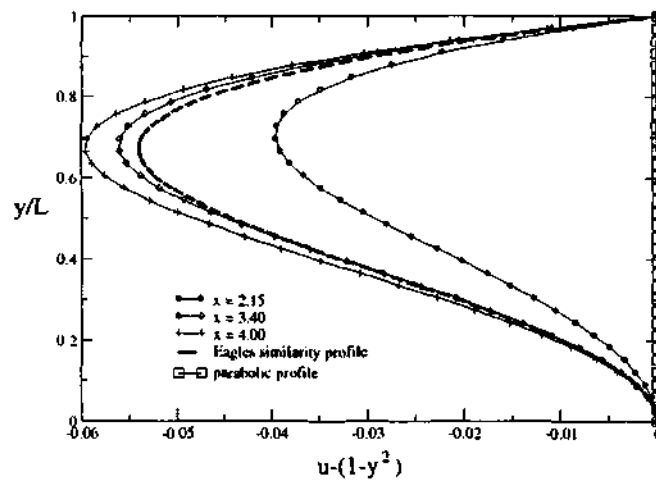

Figure 6.9: Comparison of Eagle's similarity profile with the present result, $Re = 20$ and angle of divergence $= 5^0$.

The following results from fig.(6.10) to fig.(6.14) for the flow in a divergent channel, are based on Re $= 200$, angle of divergence $\theta = 10^0$. The computational domain is 1:40 (the streamwise extent is 40 times the half channel width). For this Reynolds number, a long straight streamwise portion following the divergent section is required for the profile to develop. The separation bubble for this case can be clearly seen in fig.(6.14).
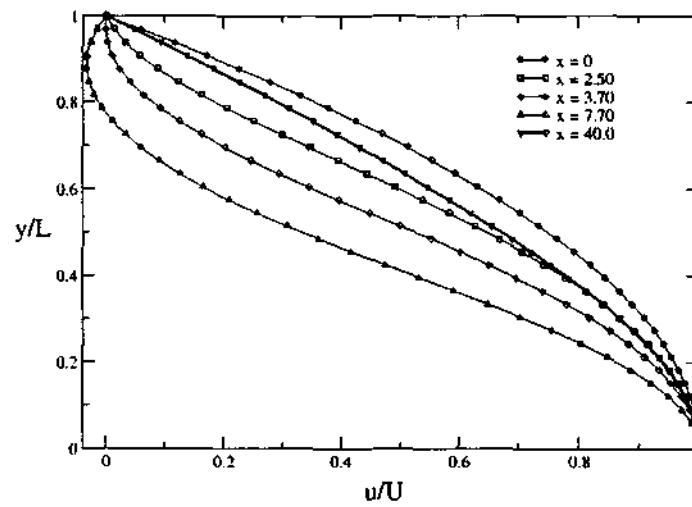

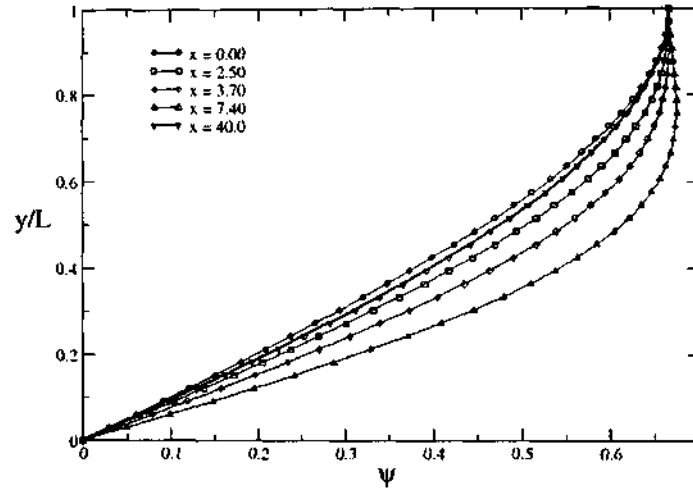Figure 6.10: Streamwise velocity profile, $Re = 200$ and angle of divergence $= 10^0$.

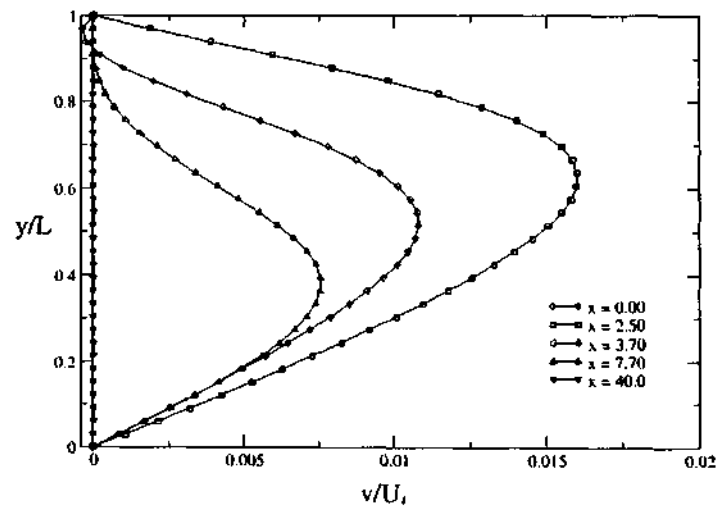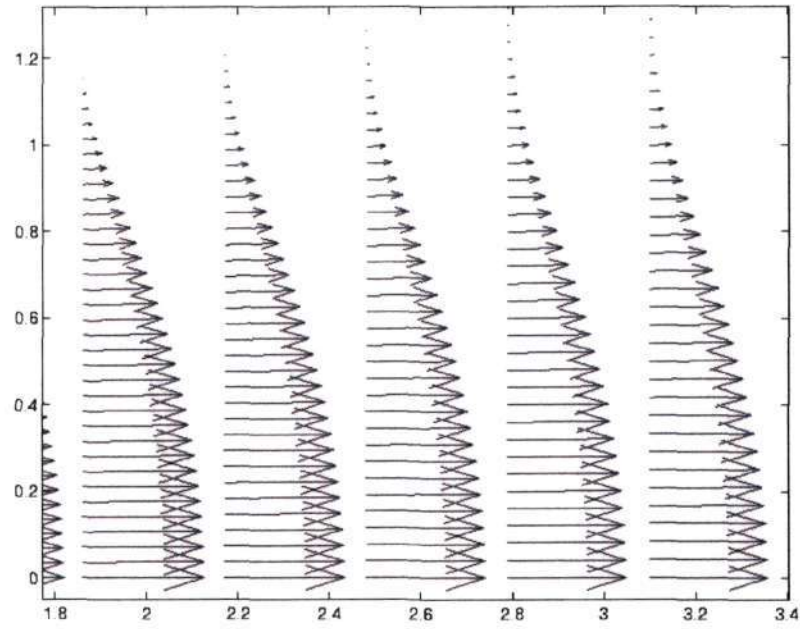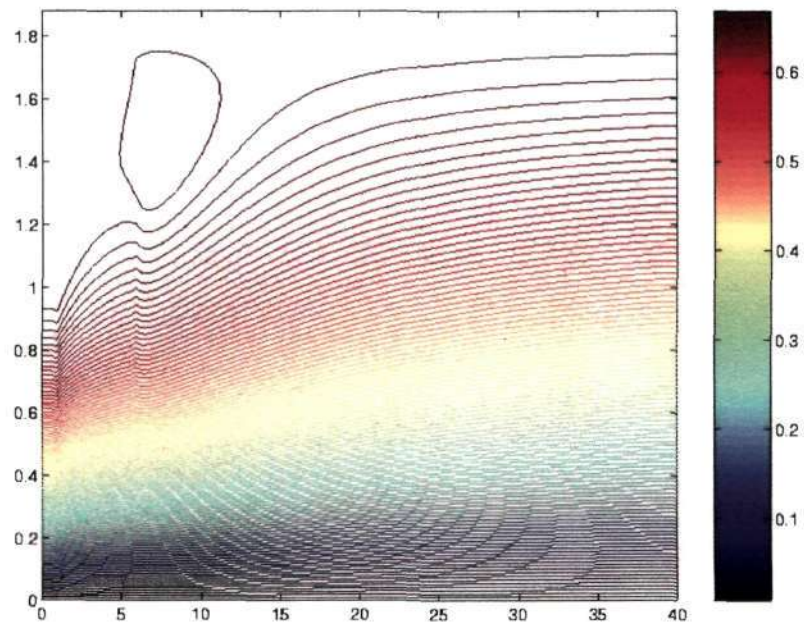Figure 6.11: Streamfunction contour at steady state, $Re = 200$ and angle of divergence $= 10^0$.

Figure 6.12: Normal velocity profile at steady state, $Re = 200$ and angle of divergence $= 10^0$.

Figure 6.13: $Re = 200$ and angle of divergence $= 10^0$.

Figure 6.14: Streamline of the flow, $Re = 200$ and angle of divergence $= 10^0$.

6.2   Results: Axisymmetric flow

The geometry for the axisymmetric flow in a divergent pipe is shown in fig.(6.15). The results are based on $Re = 50$ and angle of divergence $\theta = 5^0$. The computational domain is 1:100. It can be seen from the fig.(6.15), the exit portion is large enough, to ensure that the exit boundary condition is accurately specified.
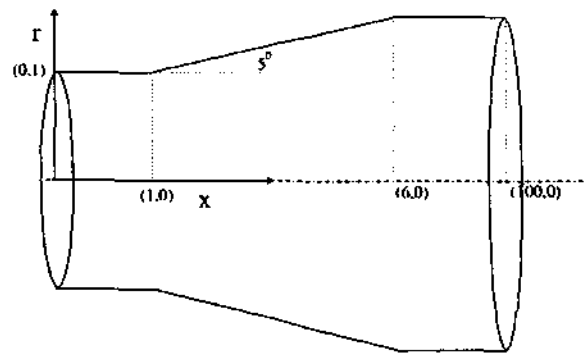

Figure 6.15: Physical domain for the axisymmetric flow in a pipe, figure is not scaled.

The convergence behaviour of vorticity residual are shown in fig.6.16. It can be seen that the convergence of vorticity residual is exponential all the way down to an error of 10^{-6}. The streamwise velocity profiles at different locations in the downstream are shown in fig.(6.17). The flow is separated at $x = 4.615$ and again reattached at about $x = 10$, giving unchanged parabolic profiles after 92.3. The corresponding normal velocity, streamfunction and

vorticity profiles are shown in fig.(6.18), fig.(6.19) and fig.(6.20) respectively. As one would intutively expect, divergence produces a flow separation more easily in an axisymmetric flow than in a channel.
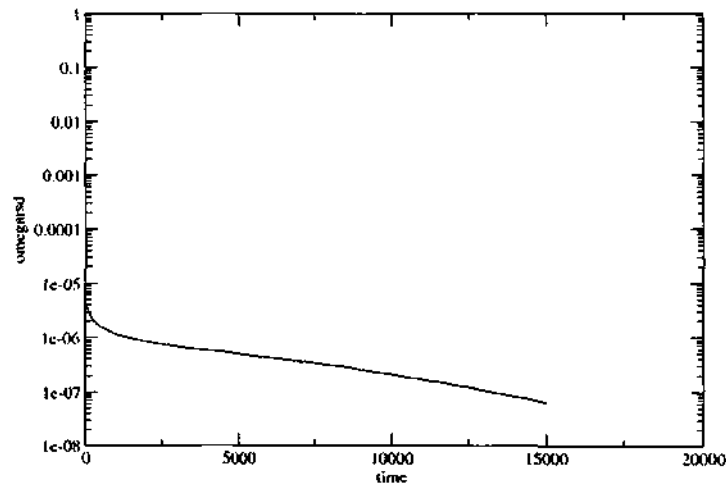

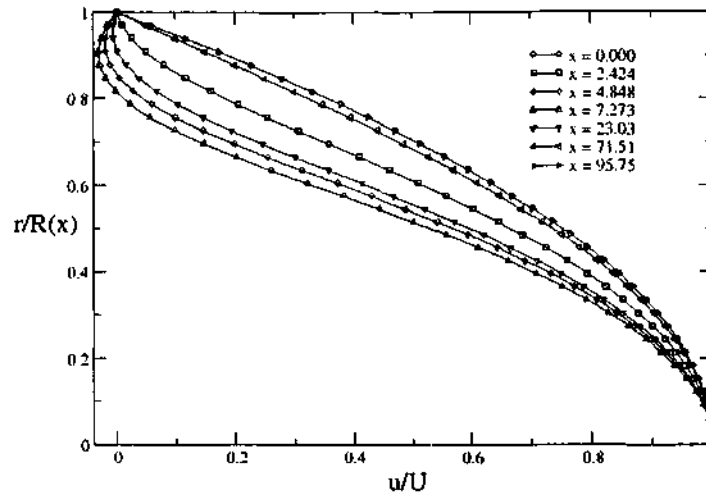Figure 6.16: ω_{rsd} Vs time, $Re = 50$ and angle of divergence $= 5^0$.

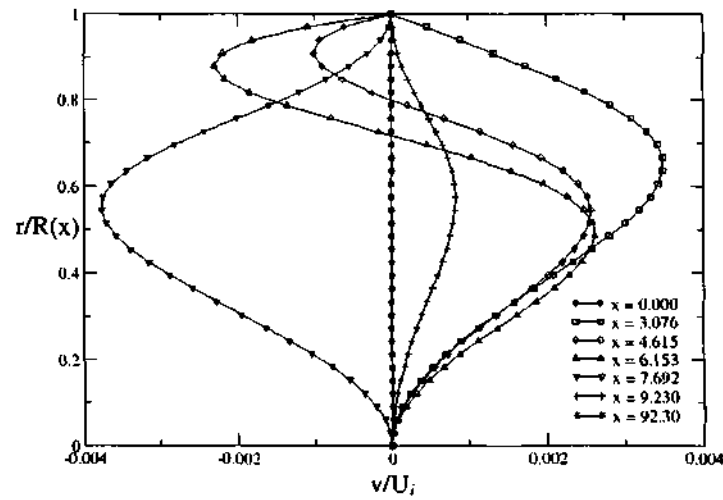Figure 6.17: Streamwise velocity profile, $Re = 50$ and angle of divergence $= 5^0$.

Figure 6.18: Normal velocity profile, $Re = 50$ and angle of divergence $= 5^0$.
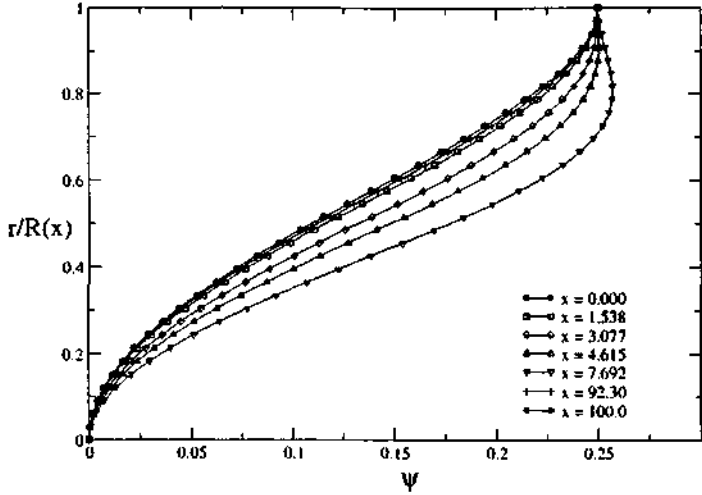
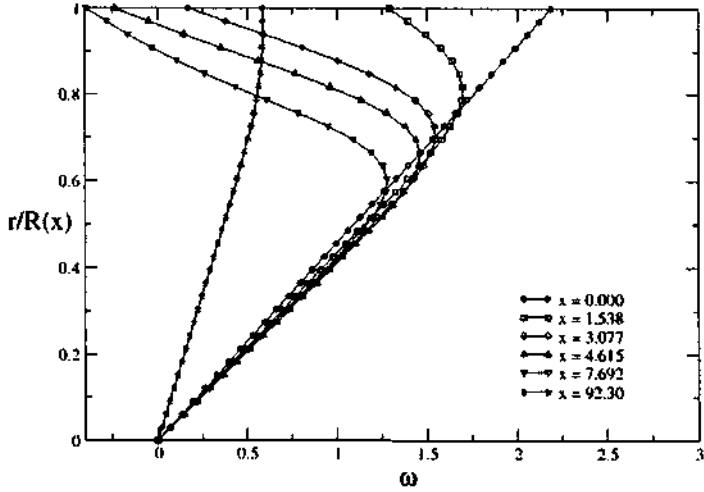Figure 6.19: Streamfunction contour at steady state, $Re = 50$ and angle of divergence $= 5^0$.

Figure 6.20: Vorticity profile at steady state, $Re = 50$ and angle of divergence $= 5^0$.

Chapter 7

Conclusions and Scope for Future Work

A general code for spatially developing 2D incompressible flow has been developed, using the Navier-Stokes equation in the vorticity and streamfunction formulation. The Gauss-Seidel technique was found to be alarmingly slow in solving the elliptic streamfunction and vorticity equation with vorticity as a source term, as in case if spatially developing flow large computational domain is required. To accelerate the rate of convergence a full-multigrid algorithm has been implemented. The present code has been validated with a number of experimental and theoretical known results, like developing flow in a plane channel and flow in a backward-facing step. The full-multigrid algorithm has been compared with the Gauss-Seidel technique for heat conduction equation. The code has been used to simulate the separated flow with reattachment for divergent channel and pipe, with a straight exit portion for different angles of divergence and Reynolds numbers. Although it

has been used for the flow in simple geometry like divergent channel and pipe for the present work, it can be used for complex geometry as well. The code in the present form can handle unsteady problems, but has been used up to now to solve pseudo-unsteady problems to obtain steady state solutions. The limitation of the code in the present form is that it cannot be used for cases where a straight forward transformation into a simple computational domain is not possible.

As already explained, Eagles [1] used the similarity flow profile for the stability of slowly varying divergent channel. But for flow in a divergent channel, with large angle of divergence a similarity solution may not be be valid, because the streamwise diffusion term is not small. The stability of such flow needs a non-parallel stability analysis with a correct flow profile. The present code can be used for getting the required velocities profiles. In summary, now we have the capability of studying the stability and unsteadiness of wide class of spatially developing and pulsatile flows.

Bibliography

[1] P. Eagles and M. Weissman, "On the stability of slowly varying flow: the divergent channel," *J. Fluid Mech.*, vol. 69, pp. 241–262, 1975.

[2] J. D. Anderson, *Computational Fluid Dynamics.* McGraw-Hill, Inc.

[3] P. Eagles, "The stability of a family of jeffer-hamel solutions for divergent channel flow," *J. Fluid Mech.*, vol. 24, pp. 191–207, 1965.

[4] P. Eagles, "Supercritical flow in a divergent channel," *J. Fluid Mech.*, vol. 57, pp. 149–160, 1972.

[5] R. L. Panton, *Incompressible flow.* Springer.

[6] F. W. White, *Viscous Fluid Flow.* McGraw-Hill, Inc., 2nd ed. ed., 1991.

[7] C.A.J.Fletcher, *Computational Techniques for Fluid Dynamics*, vol. I. Springer, 2nd ed. ed.

[8] C.A.J.Fletcher, *Computational Techniques for Fluid Dynamics*, vol. II. Springer, 2nd ed. ed.

[9] S. Vanka *Private communication*, 2003.

[10] P. J. Roache, *Computational Techniques for Fluid Dynamics.* Springer.

[11] J. H. F. Peric, *Computational Techniques for Fluid Dynamics*. Springer.

[12] M. B. Dogruoz, "CFD benchmark testing of selected laminar flow problems," vol. http://w3.arizona.edu/ thermlab/, Octobor 7, 2002.

[13] M. V. Dyke, "Entry flow in a channel," *J. Fluid Mech.*, vol. 44, pp. 813–823, 1970.

[14] B. F. Armaly and F. Durst, "Experimental and theoretical investigation of backward-facing step flow," *J. Fluid Mech.*, vol. 127, pp. 473–496, 1983.